Received: 22 November 2021 | Revised: 7 February 2022 | Accepted: 8 February 2022

DOI: 10.1002/pol.20210853

RESEARCH ARTICLE

JOURNAL OF POLYMER SCIENCE WILEY

Uniform antibacterial cylindrical nanoparticles for enhancing the strength of nanocomposite hydrogels

Zehua Li[1,2,3] | **Amanda K. Pearce**[2] | **Jianzhong Du**[3] | **Andrew P. Dove**[2] | **Rachel K. O'Reilly**[2]

[1]Department of Chemistry, University of Warwick, Coventry, UK

[2]School of Chemistry, University of Birmingham, Birmingham, UK

[3]Department of Polymeric Materials, School of Materials Science and Engineering, Tongji University, Shanghai, China

Correspondence

Jianzhong Du, Department of Polymeric Materials, School of Materials Science and Engineering, Tongji University, Shanghai, China.
Email: jzdu@tongji.edu.cn

Andrew P. Dove and Rachel K. O'Reilly, School of Chemistry, University of Birmingham, B15 2TT, Edgbaston, Birmingham, UK.
Email: a.dove@bham.ac.uk and r.oreilly@bham.ac.uk

Funding information

China Scholarship Council; Education and Scientific Research Project of Shanghai, Grant/Award Number: 21520710100; National Outstanding Youth Science Fund Project of National Natural Science Foundation of China, Grant/Award Number: 21925505

Abstract

Crystallization-driven self-assembly (CDSA) was employed for the preparation of monodisperse cationic cylindrical nanoparticles with controllable sizes, which were subsequently explored for their effect on antibacterial activity and the mechanical properties of nanocomposite hydrogels. Poly(ϵ-caprolactone)-*block*-poly(methyl methacrylate)-*block*-poly[2-(tert-butylamino) ethyl methacrylate] (PCL-*b*-PMMA-*b*-PTA) triblock copolymers were synthesized using combined ring-opening and RAFT polymerizations, and then self-assembled into polycationic cylindrical micelles with controllable lengths by epitaxial growth. The polycationic cylinders exhibited intrinsic cell-type-dependent antibacterial capabilities against gram-positive and gram-negative bacteria under physiological conditions, without quaternization or loading of any additional antibiotics. Furthermore, when the cylinders were combined into anionic alginate hydrogel networks, the mechanical response of the hydrogel composite was tunable and enhanced up to 51%, suggesting that cationic polymer fibers with controlled lengths are promising mimics of the fibrous structures in natural extracellular matrix to support scaffolds. Overall, this polymer fiber/hydrogel nanocomposite shows potential as an injectable antibacterial biomaterial, with possible application in implant materials as bacteriostatic agents or bactericides against various infections.

KEYWORDS

alginate hydrogels, antibacterial micelles, crystallization-driven self-assembly, nanocomposites

1 | INTRODUCTION

Bacterial infectious diseases represent an area of extensive health concerns, due to their high prevalence and the growing resistance of bacteria. Although conventional antibiotics are constantly being developed and updated, long-term use of these agents have caused bacteria to generate antimicrobial resistance (AMR). To overcome AMR issues, different antimicrobial agents with varied mechanisms of action have emerged,[1] which include silver nanoparticles,[2,3] metal oxide nanoparticles,[4,5] antimicrobial polymers,[6,7] and antimicrobial peptides.[8,9] Among

these agents, nanoparticles have become promising replacements of antibiotics on account of their high-surface area and reactivity, often exhibiting enhanced inhibition of the growth and reproduction of bacteria in comparison with traditional antibiotics.[7] However, inorganic-based nanoparticles can lead to potential side effects in vivo, where their metabolism, clearance, and cytotoxicity are still being studied.[10] Therefore, organic antibacterial block copolymers (BCPs) and their nanoscale assemblies are alternative low-cost choices, and as such have been widely investigated for their prolonged antibacterial activity,[11] improved antibiotic resistance,[12] and low cytotoxicity.[13]

One class of antibacterial polymers feature cationic groups, yielding polycationic nanostructures with a high-charge density after assembly that can easily rupture the bacterial membrane.[14] The antibacterial activities of polycationic nanoparticles can be tuned by altering the chemistry, dimension, morphology, and surface charge of the micelles.[15–17] Previously, the effect of micelle shape and size on the antimicrobial activities of quaternized polymeric nanoparticles assembled through crystallization-driven self-assembly (CDSA) was explored, where the small 2D rhombic platelets exhibited higher antibacterial activities than larger platelets, spheres, and unassembled polymers.[17] However, the required quaternization process generated quaternary ammonium compounds, which can lead to hemolysis and thus limits further biomedical application.[7] To overcome this limitation, cationic polymers without quaternary nitrogen atoms have also been investigated, such as poly[2-(*tert*-butylamino) ethyl methacrylate] (PTA).[18–20] Of importance, this polymer has demonstrated high antibacterial activity against both gram-positive and gram-negative bacteria, but low cytotoxicity to human cells.[21,22] The antimicrobial mechanism of PTA is attributed to its pendant secondary amine groups, which have a pKa of 9.12 and so can be positively charged in neutral water. This allows PTA to exchange the Ca^{2+} or/and Mg^{2+} cations and destroy the integrity of the lipopolysaccharides in the outer membrane of bacteria,[23] followed by disorganization and subsequent bacterial apoptosis.[18,22,24] Furthermore, PTA is both partially hydrophilic and partially hydrophobic in neutral water, and thus is able to penetrate through the cell wall/membrane of bacteria.[22] Therefore, in comparison with other amine-containing cationic polymers, PTA shows antibacterial capabilities without the need for quaternization.[21,22,24]

According to the aforementioned advantages, PTA and its block copolymers have been considered as effective additives to confer antimicrobial abilities to polymeric composites,[25,26] polymer films,[21] and polymeric nanoscale assemblies.[22,24,27] Unlike common antibacterial polymer composites and films, PTA-based block copolymers can self-assemble into secondary nanostructures, which can result in enhanced antimicrobial properties.[22] Du and coworkers synthesized PTA-based triblock copolymers to form biodegradable and antibacterial polymer micelles that did not require quaternization.[22] They demonstrated that the MIC of these PTA-based micelles were cell-type-dependent, where MIC values were lower against *Staphylococcus aureus* (*S. aureus*) compared with *Escherichia coli* (*E. coli*), regardless of PTA content. Furthermore, they further reported PTA-based diblock copolymers that could be self-assembled into polymer vesicles in water upon increasing the temperature, demonstrating excellent antibacterial efficacy without quaternization. When treated with 0.25 mg ml^{-1} vesicles, 99.9% and 99.8% *E. coli* and *S. aureus* were killed, respectively.[24] Song et al. employed PTA polymers as a coating on the surface of silica nanoparticles, where their antimicrobial activities were dependent upon the nanostructure size, as well as bacteria strain.[27] They observed that 17 nm core-shell spheres showed the lowest MIC values against *E. coli* and *S. aureus* compared with their 28 nm and 50 nm particle counterparts and the bulk polymers. Although PTA has proven promising for antimicrobial applications, the influence of nanoparticle shape and of self-assembly dimensional factors, such as length of cylindrical micelles, have not been systematically studied. As a result, structure–function relationships between the cylinder size and antibacterial properties have yet to be determined. CDSA is a versatile self-assembly method that provides control over micelle morphology and dimension, and therefore offers the ideal tool to prepare low-dispersity cylindrical micelles with precisely controlled lengths for this interesting surface chemistry.[28] In addition, we have shown in previous research that the inclusion of polymer fibers can enhance the mechanical properties of alginate-derived hydrogels under shear strain.[29] However, PTA-based antimicrobial nanoparticles have not been studied in this context. Considering the anionic nature of alginate-based hydrogels,[30] PTA-based cationic cylindrical micelles should readily crosslink with the negatively charged alginate polymer chains, resulting in superior mechanical strength enhancement in comparison with blending neutral cylinders.

In this work, 2-(*tert*-butylamino)ethyl methacrylate (TA) was utilized in the synthesis of new antimicrobial ABC triblock copolymers. The resultant polymer was demonstrated to form cylindrical micelles through a 'bottom-up' CDSA approach, giving access to water-dispersible, biodegradable, and antibacterial polymer fibers with PTA groups on the corona (Scheme 1). The secondary amine on the PTA polymer backbone successfully conferred antimicrobial activity to the fibers against both gram-negative *E. coli* and gram-positive *S. aureus* bacteria

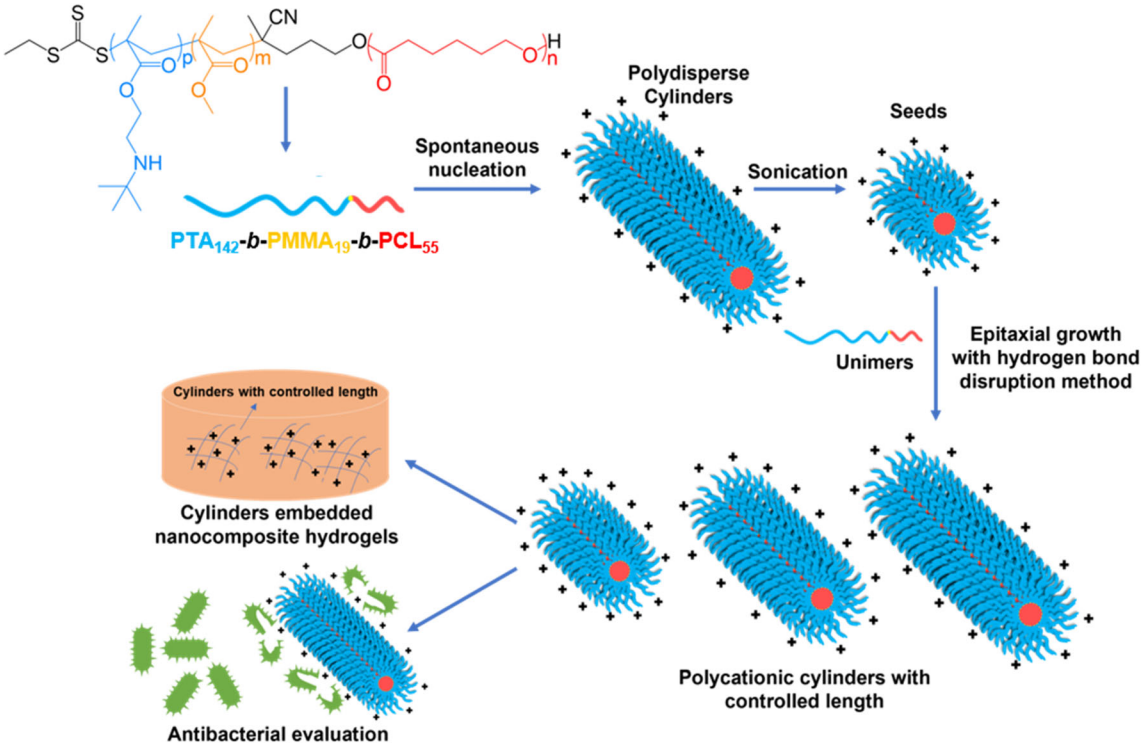

SCHEME 1 Schematic representation for the formation of PTA-based polycationic cylindrical micelles with various lengths through epitaxial growth, and the fabrication of cylinder-embedded nanocomposite hydrogels

at neutral pH, exhibiting good MIC values in the absence of quaternization or additional biocides.[24] In particular, cylinders with lengths of 500 nm and 750 nm exhibited higher antimicrobial activities than cylinders with other lengths, spheres, unassembled PTA homopolymers, and neutral cylinders. Moreover, the mechanical properties of anionic alginate hydrogels under shear strength were enhanced following incorporation of the cationic cylinders. In particular, the 500 nm cylindrical nanoparticles resulted in a significant enhancement (up to 51%) in the resistance to breaking under strain when formed into nanocomposite hydrogels, which was higher than their counterparts with other dimensions. Overall, this study demonstrates the 'bottom-up' production of antibacterial polymer fibers allowing the effect of dimensions on antibacterial properties and mechanical strength of nanocomposite hydrogels to be investigated, and highlighting the significance of controlling nanoparticle sizes in biomedical applications.

2 | RESULTS AND DISCUSSION

2.1 | Triblock copolymer synthesis and characterization

Cylindrical nanoparticles with controllable sizes were prepared in order to investigate the influence of polymeric micelle dimensions on their antibacterial activity and the ability to enhance the mechanical properties of hydrogels. According to previous research, the inclusion of poly(ϵ-caprolactone) (PCL) as the crystalline component in block copolymers can induce self-assembly to prepare cylindrical nanostructures, giving access to controlled cylindrical micelle lengths by epitaxial growth.[29] To prevent instability and disassembly of the polymer fibers in aqueous environments, resulting from the corona block swelling and the subsequent crystalline core fracture, the glassy and highly hydrophobic poly(methyl methacrylate) (PMMA) was used as an interfacial block to protect the crystalline segment.[31] To provide the active antibacterial ingredient, the corona block of the triblock copolymer was provided by the polycationic poly[2-(*tert*-butylamino)ethyl methacrylate] (PTA). Following the above strategy, poly(ϵ-caprolactone)-*block*-poly(methyl methacrylate)-*block*-poly[2-(*tert*-butylamino)ethyl methacrylate] (PCL-*b*-PMMA-*b*-PTA) triblock copolymers were obtained.

The triblock copolymers were synthesized through the ring-opening polymerization (ROP) of ϵ-caprolactone (ϵ-CL), followed by the reversible addition-fragmentation chain transfer (RAFT) polymerizations of methyl methacrylate (MMA) and 2-(*tert*-butylamino)ethyl methacrylate (TA) respectively. First, the PCL macroCTA was synthesized by the ROP of ϵ-CL in a nitrogen-filled glove box with a dual-headed initiator/chain transfer agent (CTA)

and diphenyl phosphate (DPP) as catalyst, in dry toluene at room temperature (RT) (Scheme S1A). To minimize any transesterification of the polymer backbone, the polymerization was quenched when the monomer conversion reached 83%, followed by precipitation into ice-cold diethyl ether. Successful synthesis of the PCL block was confirmed by proton nuclear magnetic resonance (^{1}H NMR) spectroscopy, where the methylene resonances on the repeat units were observed at δ = 4.06 ppm and δ = 2.30 ppm and the end group at δ = 3.65 ppm (Figure S1). By comparing the integrations of the characteristic signals and the end group, the degree of polymerization (DP) was calculated as 55, giving a molecular weight (M_n) of 6.5 kg mol^{-1} (Table S1). Size exclusion chromatography (SEC) in tetrahydrofuran (THF) eluent revealed the narrow molecular weight dispersity ($Đ_M$ = 1.06, PMMA standards, Table S1, Figure S4A) of the PCL homopolymer, indicating a well-controlled living polymerization. Importantly, the retention of the trithiocarbonate end group was observed by the SEC UV–Vis detector at λ = 309 nm (Figure S4B), and the absence of transesterification and water initiation were observed by matrix-assisted laser desorption/ionization time of flight (MALDI ToF) mass spectrometry (Figure S5A).

To avoid disassembly of the nanoparticles in the aqueous phase and the subsequent precipitation, MMA was utilized to act as a short interfacial segment between the PCL and PTA blocks. MMA was polymerized in 1,4-dioxane at 70 °C in the presence of the PCL macro-CTA and the radical initiator 2,2-azobis(2-methylpropionitrile) (AIBN) (Scheme S1B). After 5 h, the reaction reached 40% conversion, and was purified by precipitation into ice-cold methanol to obtain the PCL-*b*-PMMA diblock copolymer. The successful polymerization was confirmed by ^{1}H NMR spectroscopic analysis using the methyl resonances of the PMMA repeat units at δ = 3.59 ppm and δ = 1.02 ppm (Figure S2). The DP of PMMA was calculated to be 19, and thus the M_n of the diblock copolymer was 8.4 kg mol^{-1}. SEC analysis with THF as eluent revealed a monomodal and narrow distribution ($Đ_M$ = 1.07, PMMA standards, Table S1, Figure S4A), and the UV–Vis detector at λ = 309 nm demonstrated the retention of the trithiocarbonate end group on the diblock copolymer (Figure S4B). Finally, synthesis of the PTA block was performed using the PCL-*b*-PMMA macro-CTA in 1,4-dioxane at 70 °C with AIBN as the radical initiator (Scheme S1C). The reaction was quenched after 24 h once monomer conversion reached 71% as determined by ^{1}H NMR spectroscopy (to ensure fidelity of the RAFT end groups) by precipitation into ice-cold methanol. Successful polymerization of the PCL-*b*-PMMA-*b*-PTA triblock copolymer was confirmed using the methyl resonance of the PTA repeat units observed at δ = 1.11 ppm and the methylene resonances at δ = 2.79 and δ = 4.02 ppm (Figure S3), giving a calculated DP of 142 and a M_n of 34.7 kg mol^{-1}. SEC analysis with THF as eluent showed a low-overall polymer dispersity with a clear molecular weight shift after each block, no evidence of a low-molecular weight species ($Đ_M$ = 1.12, PMMA standards, Table S1, Figure S4A), and the retention of the trithiocarbonate end group as confirmed via the UV detector at λ = 309 nm (Figure S4B). Importantly, the absence of any unreacted PCL homopolymer or/and PCL-*b*-PMMA diblock copolymer was confirmed by diffusion-ordered spectroscopy (DOSY) NMR analysis, where a single diffusion coefficient was observed in the measured spectrum correlating with the polymer peaks (Figure S5B,C).

2.2 | Crystallization-driven self-assembly for the production of cylindrical micelles

Cylindrical nanoparticles of controlled sizes were prepared in order to investigate the effect of nanoparticle dimensions on antibacterial activities and the mechanical strength of nanocomposite hydrogels. First, using the spontaneous nucleation method as previously reported,[29,31] the PCL_{55}-*b*-$PMMA_{19}$-*b*-PTA_{142} triblock copolymer was used to prepare polydisperse cylindrical micelles (Figure 1A, Figure 1B a). The triblock copolymer was heated at 5 mg ml^{-1} in ethanol for 4 h at 90 °C without stirring, before cooling to RT. The crystalline nature of the formed polymer fibers was confirmed through wide angle x-ray scattering (WAXS) analysis, with 2theta (2θ) peaks of the crystalline PCL block at ca. 21° and 24° (Figure S6).[32]

Subsequently, monodisperse micelles with controllable dimensions were prepared using a living CDSA method called epitaxial growth. In this process, uniform crystalline seeds are prepared by probe sonication of the polydisperse cylinders, exposing the crystalline terminus of the resultant particles to act as sites for further epitaxial growth of free triblock copolymers (unimer) in the selected solvent, analogous to a living polymerization.[33] Low dispersity nanoparticles of precise sizes can be obtained simply through controlling the addition of unimers. In this study, an undesirable congregation of unimers occurred following addition to the seed solutions. We hypothesized this was the result of formation of intermolecular N − H···N hydrogen bonds (HBs) between the secondary amine groups on different PTA chains, leading to the limited movement of macromolecules and the congregation of unimers, thereby restricting the PCL crystalline process. To overcome the potential HBs interaction, the HBs disruption agent 2,2,2-trifluoroethan-1-ol (trifluoroethanol, TFE) was added into the selective solvent system.[34]

In line with the procedure described above, the PCL_{55}-*b*-$PMMA_{19}$-*b*-PTA_{142} triblock copolymer polydisperse

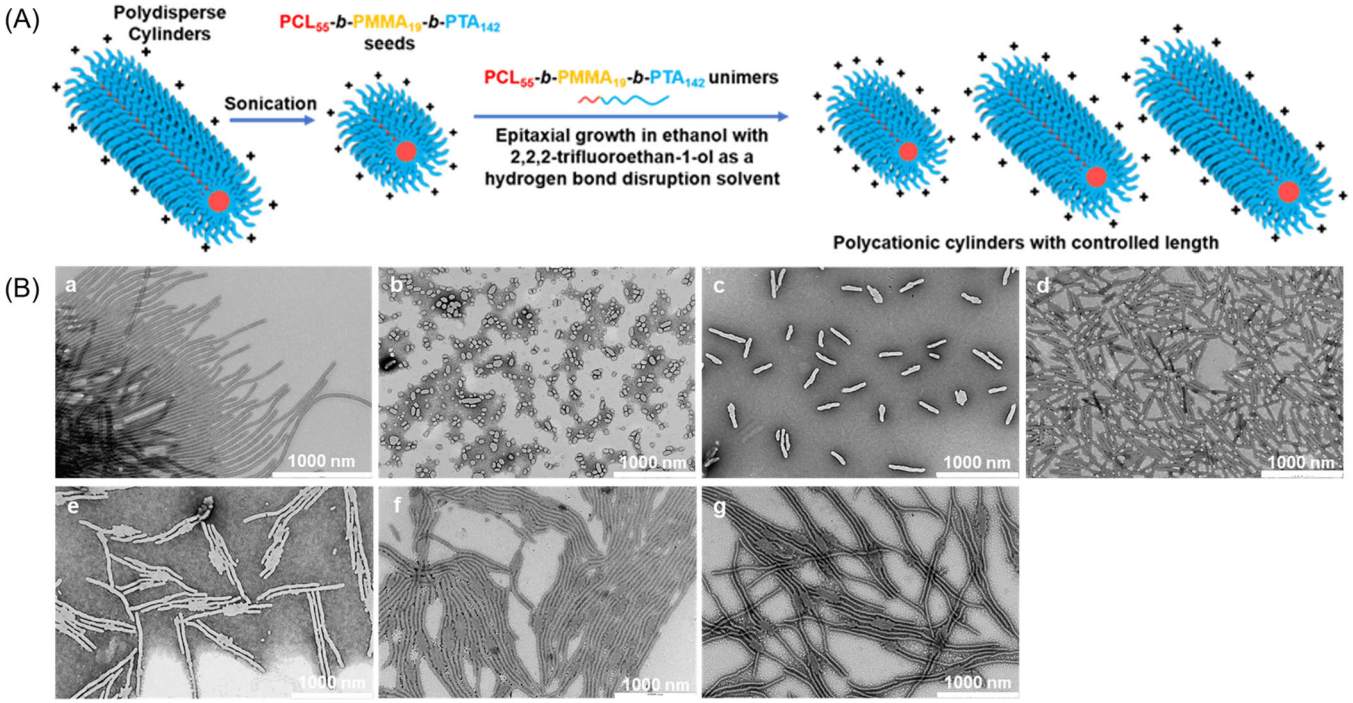

FIGURE 1 (A) Schematic of epitaxial growth of PCL_{55}-*b*-$PMMA_{19}$-*b*-PTA_{142} cylindrical micelles in ethanol from 68 nm seeds. (B) Transmission electron microscopy (TEM) micrographs of (a) polydisperse cylinders, (B) monodisperse seeds, and the epitaxial growth of cylinders in TFE/EtOH mixed selective solvent (volume ratios of 2:98) at 3 °C targeting (C) 235 nm (D) 500 nm, (E) 748 nm, (F) 1428 nm, (G) 2108 nm length values. 1 wt% uranyl acetate was used as a negative stain. Scale bar = 1 μm

micelles (Figure 1B a, 0.5 mg ml^{-1}) in ethanol were treated with probe sonication to prepare seed micelles. The sonication was carried out under controlled temperature at 0 °C, where the total 40 min process was divided into 20 rounds. The micelle solution was cooled in an ice bath for at least 10 min between each round to prevent undesired crystallization caused by local high temperatures. After the sonication treatment, low dispersity seed micelles were obtained, with a number average length of ca. 68 nm (Figure 1B b, Figure 2B).

For the living CDSA procedure, a unimer solution of 100 mg ml^{-1} was prepared by dissolving the PCL_{55}-*b*-$PMMA_{19}$-*b*-PTA_{142} triblock copolymer in *N,N*-dimethylformamide (DMF), as a good solvent for the triblock copolymers that was miscible with the TFE/EtOH corona-selective solvent. The seed solution, in TFE/EtOH with a volume ratio of 2:98, was precooled to 3 °C before the addition of unimer solutions with unimer-to-seed mass ratios of 3.5, 7.4, 11.0, 21.0, and 31.0 to target different length cylindrical micelles, followed by manually shaking for 10 s and aging at 3 °C for 2 weeks to obtain stable structures.

The growth of cylindrical micelles could be visually observed, with solutions of longer cylinders exhibiting more turbidity. The controlled linear epitaxial growth process was confirmed by TEM, where the precise lengths of low-dispersity cylindrical micelle bundles were predictable and could reach micrometers in length (Figure 1B b–g, Figure 2B) in proportion to the amount of added unimers (Figure 2A, Figure 2C). The final monodisperse polymer fiber bundles with precise lengths were transferred into an aqueous solution by dialysis against water for 72 h to allow for subsequent gelation and antimicrobial studies. After dialysis, the nanoparticles were confirmed to still exhibit stable cylinder bundle structures without disassembly or degradation (Figure S7). The cationic nature of the PTA-based assembled cylinders due to the tert-butylamino group on the PTA block (pKa 9.12)[22,24] being positively charged in neutral water was confirmed by zeta-potential (ζ-potential) measurements, which were found to be higher than +30 mV for all cylinders (Table S2).

2.3 | Conventional self-assembly in solution of the triblock copolymer

To further understand the role of nanoparticle shape in the resultant properties, such as antibacterial activity and mechanical strength of nanocomposite hydrogels, spherical micelles were prepared as a control using a conventional self-assembly method in solution. For

(A)

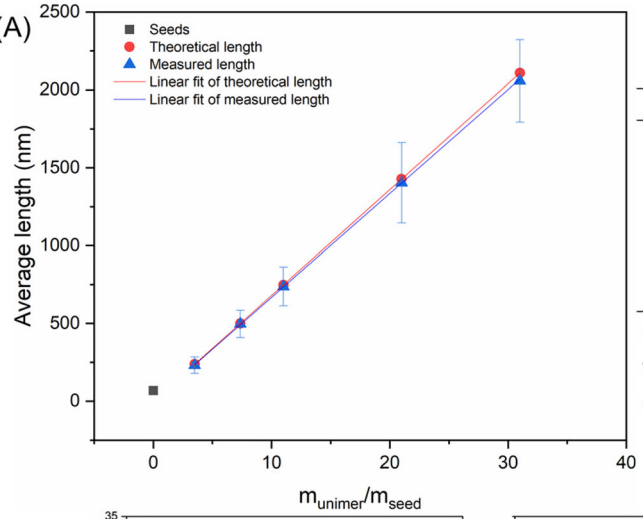

(B)

Target (nm)	L_w[a] (nm)	L_n[b] (nm)	L_w/L_n
Seeds	70	68	1.03
238	244	232	1.05
500	512	497	1.03
748	758	737	1.03
1428	1452	1404	1.03
2108	2087	2053	1.02

Imaged by TEM; one hundred cylinders per sample were counted to measure the length of cylinders by ImageJ. [a] L_w = weight average length. [b] L_n = number average length.

(C)

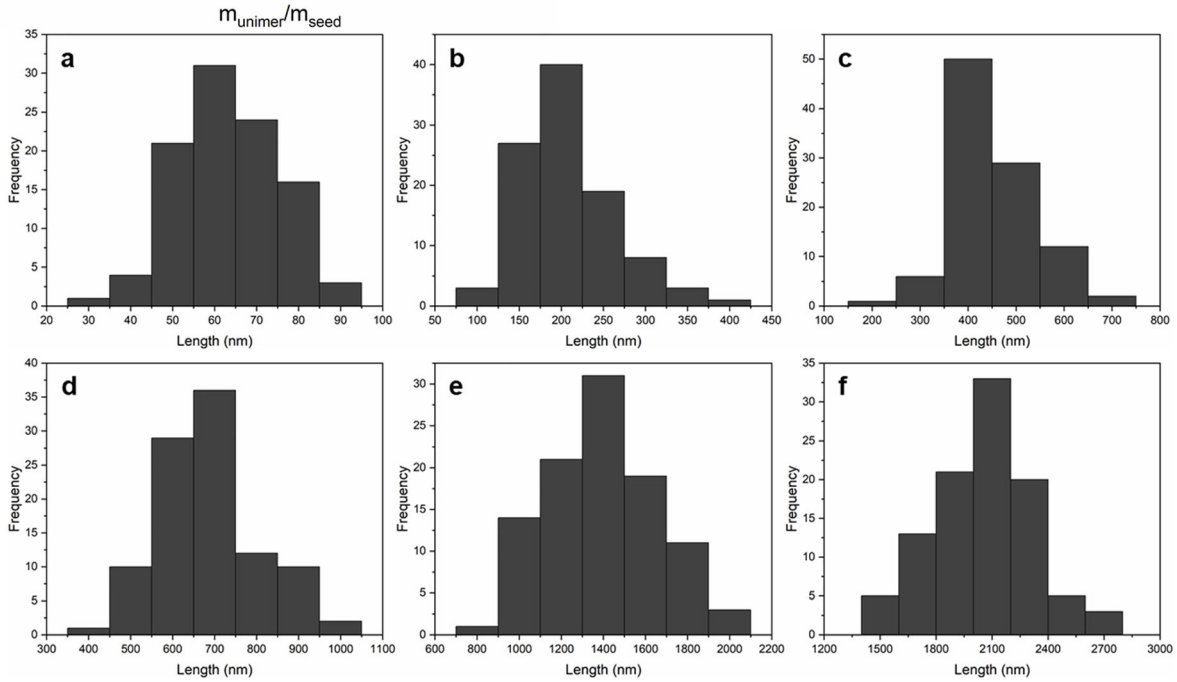

FIGURE 2 (A) Linear epitaxial growth of PCL_{55}-*b*-$PMMA_{19}$-*b*-PTA_{142} cylinders with narrow length dispersity (blue triangles, error bars represented the standard deviation [σ] of the length distribution) in comparison to the theoretical length (red circles), where the cylindrical micelles were grown from ca. 68 nm seeds. (B) Length dispersity of cylindrical micelles formed by epitaxial growth of PCL_{55}-*b*-$PMMA_{19}$-*b*-PTA_{142} cylindrical micelles. (C) Diameter distribution of (a) seeds, (B) 235 nm cylinders, (C) 500 nm cylinders, (D) 748 nm cylinders, (E) 1428 nm cylinders, and (F) 2108 nm cylinders

this, a solvent switch method was used, whereby the PCL_{55}-*b*-$PMMA_{19}$-*b*-PTA_{142} triblock copolymer was dissolved in a common solvent (THF), followed by the slow addition of an excess of ultrapure water (18.2 MΩ·cm) through a syringe pump and finally exhaustive dialysis against ultrapure water to remove the organic solvent.[35]

After dialysis, dynamic light scattering (DLS) and TEM were used to characterize the size and morphology of the spheres. DLS analysis of a 1 mg ml^{-1} dispersion of particles in ultrapure water showed a unimodal population by number, volume, and intensity (Figure S8A,B), with a diameter of 162.6 nm and a polydispersity index (PDI) of 0.107 (Table S3). TEM images showed the presence of aggregates of spherical micelles with a size of ca. 160 nm (Figure S8C). However, the diameter of the individual micelles was calculated as ca. 23 nm by counting one hundred spheres to measure by ImageJ. Therefore, the large DLS result was attributed to the aggregation of spheres caused by HBs between the secondary amines on the corona chains. Zeta-potential measurements confirmed the cationic character of the spherical nanoparticles (Table S3).

2.4 | Mechanical properties of the nanocomposite hydrogels

Next, the relationship between the size of the cylindrical micelle bundles and the resultant mechanical strength of the nanocomposite hydrogels was studied. A calcium-alginate hydrogel network system was chosen as the matrix because of its good biocompatibility, facile processing approach, low-mechanical strength, and prospects in translational medicine. It is well known that the alginate hydrogel system is negatively charged due to the presence of carboxylic acid groups, and can form a gel through crosslinking with cationic molecules, such as the divalent calcium cation. The PCL_{55}-*b*-$PMMA_{19}$-*b*-PTA_{142} triblock copolymer has secondary amine groups that were theorized to physically crosslink the anionic alginate network. As such, in comparison with our previous work the neutral cylinders,[29] the cationic cylinders should, in theory, better enhance the mechanical properties of the nanocomposite hydrogels.

Calcium-alginate hydrogels without nanofillers were considered as the control group and were prepared by the combination of sodium alginate (1.5 wt%), calcium carbonate ($CaCO_3$, 0.5 eq.), and D-glucono-δ-lactone (GDL, 1.0 eq.). During the gelation, the slow hydrolysis of GDL enabled uniform dispersion of the released calcium ions, giving a slower gelation time but good mechanical properties.[36] Next, the incorporation of the polycationic polymer fiber bundles with precise lengths was investigated (Figure 3A). Nanocomposite hydrogels were prepared as described above with a constant concentration of calcium for crosslinking, followed by blending with different equivalents of monodisperse PCL_{55}-*b*-$PMMA_{19}$-*b*-PTA_{142} cylindrical micelle bundles at RT.

Oscillatory rheology analyses were utilized to measure the mechanical strength of the nanocomposite hydrogels. Control groups were established in each dataset to ensure that trends were not impacted by slight variations during sample preparation, e.g., the lab temperature, which could lead to small changes in the magnitude of the theoretical moduli between datasets. The gel-like behavior of all samples was confirmed by the storage and loss modulus (G' and G''), where $G' > G''$ was observed in the entire range of the frequency sweep

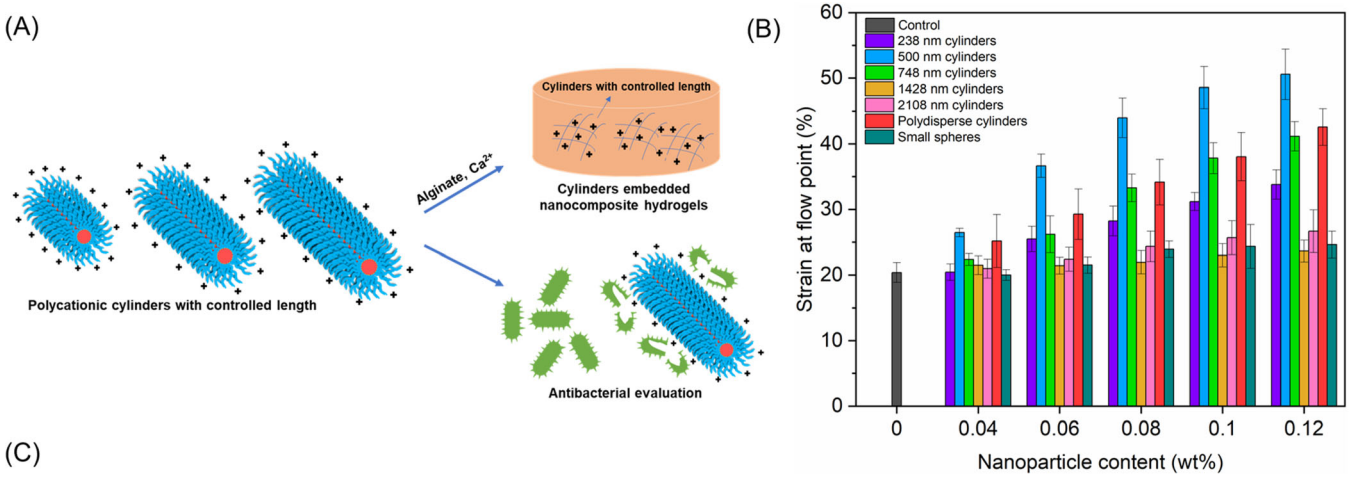

(C)

Bacteria Property		MIC (μg mL^{-1})										
Bacteria [a]	+ or - [b]	68 nm [c]	238 nm [c]	500 nm [c]	748 nm [c]	1428 nm [c]	2108 nm [c]	Polydisperse [d]	Spheres [e]	Individual polymers [f]	PDMA cylinders [g]	Ciprofloxacin [h]
S. aureus (SA01)	+	500	500	125	250	250	250	500	500	250	1000	0.125
S. aureus (SA02)	+	250	250	125	125	250	250	500	500	250	1000	8
E. coli (EC07)	-	125	250	125	125	125	125	250	500	250	1000	0.025
E. coli (EC19)	-	125	250	125	62.5	125	250	250	500	250	1000	0.5

[a] Bacteria abbreviations: *Staphylococcus aureus* (sphere-like), *Escherichia coli* (rod-like).
[b] + or - indicates Gram-positive and Gram-negative bacteria, respectively.
[c] PCL_{55}-*b*-$PMMA_{19}$-*b*-PTA_{142} cylinder bundles with different lengths of 238 nm, 500 nm, 748 nm, 1428 nm, and 2108 nm, respectively.
[d] PCL_{55}-*b*-$PMMA_{19}$-*b*-PTA_{142} polydisperse cylinder bundles were composed of mixing equal masses of cylinder bundles with different lengths.
[e] PCL_{55}-*b*-$PMMA_{19}$-*b*-PTA_{142} spheres were prepared by a solvent switch method with a diameter of 23 nm.
[f] PTA homopolymers with degree of polymerization of 141.
[g] PCL_{50}-*b*-$PMMA_{20}$-*b*-$PDMA_{200}$ triblock cylinders with a length of 500 nm was used as a negative control.
[h] Ciprofloxacin was used as a positive control.

FIGURE 3 (A) Schematic of preparing nanocomposite hydrogels and antibacterial polymeric micelles from cationic cylindrical micelles with precise lengths. (B) Histogram comparing the values of the strain at the flow point for nanocomposite hydrogels incorporating cationic cylindrical micelles at different wt%. Error bars represent the standard deviation of the data. (C) Antibacterial activities of polycationic nanostructures with PDMA-based cylinders as a negative control and ciprofloxacin as a positive control

in all attempts (Figure S9). The strain-dependent information was confirmed by the amplitude sweep, which showed the broad linear-viscoelastic (LVE) region and subsequent hydrogel network breakdown as the strain increased. Specifically, in the LVE region, with the increase of nanoparticle content, no substantial change in G' was observed, meaning a low potential for embrittlement of the nanocomposite hydrogels when loading fillers. As the strain was increased further, the intersection of the curves for G' and G'' was reached, where the strain at the flow point (τf) was determined as the crossover point ($G' = G''$, Figure S10).

From the amplitude sweep results, the control group without any nanoparticle additive showed a low strain at the flow point (ca. 20%). Upon gelation in the presence of 0.04, 0.06, 0.08, 0.10, and 0.12 wt% cylindrical micelle bundles, the flow strain was enhanced compared with the control group (Figure 3B). Statistical analyses (Table S4) of the strain at the flow point of the polymer fiber bundles with different lengths indicated a maximum enhancement up to 51% was achieved by combining 500 nm PCL_{55}-*b*-$PMMA_{19}$-*b*-PTA_{142} cylinder bundles at 0.12 wt%. This result was not only higher than its counterparts with other lengths and the spherical samples, but was also distinctly higher than comparable 500 nm neutral cylindrical samples, which were only enhanced by ca. 37%.[29] This phenomenon was attributed to the positive charge of the cationic cylinder bundles in water. Importantly, these results further confirmed our hypothesis in our previous study, whereby the strain of nanocomposite hydrogels was related to the pore size of the calcium-alginate hydrogels, and thus ca. 500 nm cylindrical micelles could better pack into the hydrogel pores.

For the 500 nm additives, with first addition of nanoparticles, the strain at the flow point was initially dramatically enhanced, followed by a steady climb as the content was further increased. This trend was attributed to steric hindrance, where the redundant cylinder bundles could not pack into the hydrogel pores, hence reducing the homogeneity and hindering the improvement of mechanical properties. Additionally, considering the micelles were positively charged, an overloaded cationic charge could also result in reduced crosslinking efficiency and a reduced efficiency in enhancing the mechanical properties of the gel. In contrast, the strain values of nanocomposite hydrogels blended with the 238 nm cylinder bundles and small spherical micelles were lower than for the 500 nm samples, likely as the shorter cylinders or small spheres were unable to effectively connect and crosslink in the larger pores of the calcium-alginate hydrogels. When the longer 1428 nm and 2108 nm cylinder bundles were added, no significant enhancement on the shear strength was observed, even as the nanoparticle content was increased. We ascribed this phenomenon to the steric hindrance caused by large dimensions of the cylinders disrupting the formation of hydrogel networks and thus decreasing the gel homogeneity. Notably, a sample of polydisperse cylinder bundles comprised by mixing equal masses of cylinder bundles with different lengths showed a robust enhancement in the hydrogel strain. This result was second only to the 500 nm samples, and thus confirmed the essential role of the 500 nm cylinder bundles in enhancing the mechanical properties of calcium-alginate hydrogels.

From the above, tuning the dimensions of added polymer fiber bundles was shown to regulate the mechanical strength of the nanocomposite hydrogels. In addition, the cationic properties of these cylinders could better improve the performance of hydrogels compared with neutral micelles of a similar size. Comparing the size, cationic cylinder bundles less than 750 nm in length could significantly contribute to the mechanical resistance to shear as a consequence of their good dispersion throughout the gel network. In contrast, further increasing the cylinder length to 1428 nm and 2108 nm did not show enhancement of the mechanical properties, likely due to steric hindrance of the bigger micelles. Moreover, the small sphere nanocomposites were also lower than most of the cylinder bundle samples which was attributed to differences in both morphology and size, where the zero dimension structures could not effectively connect the hydrogel network. Overall, the mechanical properties of nanocomposite hydrogels could be tuned by controlling the morphology and size of micelles, providing a model for the further design of biomimetic fibrillar hydrogels.

2.5 | Antibacterial evaluations of the cationic cylindrical micelles

Poly[2-(tert-butylaminoethyl) methacrylate] (PTA) is a polycationic polymer in neutral water (pKa 9.12), exhibiting relatively high-antibacterial activity and low toxicity to human cells.[18–20] Self-assembled cationic polymeric nanostructures have previously shown antibacterial activity through their increased charge density, increasing interactions with the microbial membrane.[14,37] Additionally, the modification of several nanoparticle properties such as dimension, morphology, surface charge, and chemistry have also shown improvement of antibacterial activities.[15,16] In this study, the use of CDSA to form PTA-based polymer micelle bundles enabled precise length control as a result of epitaxial growth, thus providing an

ideal method to investigate the relationship between micelle length and corresponding antibacterial activity.

The cationic cylindrical polymeric micelles were expected to exhibit more efficient interactions with the bacterial membrane compared with the cationic spherical micelles or non-assembled polymer chains due to the increased cationic charges of the cylindrical morphology, which plays a significant role in the disintegration of the bacterial membrane through electroporation or the sinking raft model.[38] In addition, the greater surface area of cylindrical structures could potentially lead to more effective interactions with the bacteria membrane and subsequent disintegration in comparison with their spherical counterparts or the individual molecules, and thus improved antimicrobial activities.[14] To understand the relationship between the length of polycationic cylindrical micelles and their antibacterial properties, all samples were analyzed for their activity against *E. coli* and *S. aureus* as gram-negative and gram-positive bacteria, respectively.

The minimal inhibitory concentration (MIC) was utilized to evaluate the bacteriostatic activity of polycationic cylindrical micelle bundles, where the MIC was defined as the minimum concentration of the test sample at which no visible growth of microbes was observed. The MIC assay was carried out using a broth microdilution method, with serial dilutions of each test sample to assess bacterial growth in comparison to positive (ciprofloxacin) and negative (broth only) controls. Results were determined after overnight incubation at 37 °C, by measuring the optical density in comparison to control wells of culture medium with no bacteria and bacteria with no compounds. MIC values were indicated by the lowest concentration in micrograms per milliliter that limited the development of bacterial turbidity after incubation.

As expected, the assays revealed that the cationic micelles showed bacteriostatic activities (Figure 3C), with all samples showing MIC values lower than 500 μg ml^{-1}. Specifically, against *S. aureus*, the 500 nm PTA-based nanostructures exhibited the lowest MIC results for both SA01 and SA02 bacterial strains, with MIC values of 125 μg ml^{-1}. In comparison, PTA-based cylindrical nanoparticles with both prolonged or shortened lengths had decreased antimicrobial properties. The PTA-based polydisperse cylindrical micelle bundles showed higher MIC values, suggesting an essential role of monodisperse micelles with specific sizes in the resultant antibacterial properties. The bacteriostatic properties of the nanoparticles against *E. coli* were also evaluated, where 748 nm PTA-based nanoparticles showed the lowest MIC values of 125 μg ml^{-1} against EC07 and 62.5 μg ml^{-1} against EC19, respectively. The 500 nm and 1428 nm samples also exhibited good activities, with MIC values against both EC07 and EC19 of 125 μg ml^{-1}. Their counterparts with longer or shorter micelle lengths, or the polydisperse samples, all showed higher MIC values similarly to the *S. aureus* results. Comparing the above data, the MIC values of PTA-based cylindrical micelles were cell-type-dependent, where the results against *E. coli* (rod bacterium, 1.0–2.0 μm) were generally equal or lower than *S. aureus* (spherical bacterium, up to 1 μm in diameter) under the same conditions. Typically, cationic nanoparticles have toxicities against both gram-negative and gram-positive bacteria, however, this tends to be closely related to the degree of interaction of the particles with the bacterial membrane, and therefore it is possible that the cylindrical structures may exhibit an enhanced antibacterial effect against rod-like bacteria compared to spherical bacteria due to the greater potential for cell-surface attachment.[39]

When analyzing the PTA-based spherical micelles, the MIC values against both *S. aureus* and *E. coli* were 500 μg ml^{-1}, showing lower bacteriostatic activities than the cylindrical samples. This phenomenon could be attributed to the higher surface curvature of the spherical micelles compared to cylindrical micelles, which led to less effective interactions with the bacteria membrane and thus decreased antimicrobial activities. Furthermore, no notable difference in MIC was observed between the different bacteria strains, which may be the result of their small size not enabling specific interactions with varied bacterial morphologies. The MIC values of PTA homopolymers against all bacterial strains were 250 μg ml^{-1}. In this case, the individual polymers have a high degree of mobility in solution which could allow for efficient bacteria interactions, giving slightly higher MIC results with no preference for either bacteria. Finally, as expected, the neutral cylinder samples (PDMA-based cylinders)[29] of 500 nm length as a negative control exhibited the highest MIC results due to their neutral charge in water.

From the above, the bacteriostatic activity of polycationic PCL_{55}-*b*-$PMMA_{19}$-*b*-PTA_{142} cylindrical micelle bundles with controlled lengths were able to be compared. In general, the antibacterial effect of these constructs against *S. aureus* or *E. coli* appeared to vary with the nanoparticle size or morphology. The 500 nm cylinders exhibited the highest antibacterial activity against *S. aureus* strains than their counterparts with different lengths, spherical shapes, or free polymer. In comparison, the 748 nm samples showed enhanced antimicrobial activity against *E. coli* compared to other cylindrical samples, spherical micelles, or free polymer. This trend was cell-type-dependent, which could be related to the morphology and size of the bacteria.[17] Overall, this highlights that control over the morphology and size of polycationic micelles can tune the specific bacteriostatic properties, providing proof-of-concept data towards the future design of antibacterial nanocomposites.

3 | CONCLUSIONS

In this study, the preparation of a range of polycationic cylindrical micelle bundles with controlled lengths based on a crystallizable block copolymer was investigated. Monodisperse cationic cylindrical micelles were prepared through CDSA to form cylinders of 68 nm, 238 nm, 500 nm, 748 nm, 1428 nm, and 2108 nm in length, which were subsequently tested for their antibacterial performance and improvement of the mechanical properties of calcium-alginate hydrogel matrices. Oscillatory rheology experiments showed that the cationic cylinder bundles of 238 nm, 500 nm, 748 nm in length, and polydisperse samples were all capable of enhancing the strain at the flow point of their corresponding hydrogels, where the gel strain could be enhanced by up to ca. 51% when cationic cylinders of 500 nm length were embedded. In contrast, the cationic 1428 nm and 2108 nm cylindrical samples and small cationic spheres were unable to effectively improve the gel resistance to shear strength. Overall, cationic cylindrical micelles were more effective in enhancing the properties of anionic alginate hydrogels compared with neutral polymer fibers. Antibacterial evaluation showed that the 500 nm cationic cylinder bundles exhibited the highest antibacterial activity against *S. aureus* bacteria and the 748 nm polymer fibers were the most effective against *E. coli*, while their counterparts with shorter or longer lengths had weaker antibacterial ability. Overall, the antibacterial efficacy of the PTA-based cationic micelles was cell-type-dependent, and could be related to the shape and size of the bacteria. This study has shown that the mechanical properties of nanocomposite hydrogels and the antimicrobial activities of assembled micelles can both be tuned by controlling micelle dimensions. Importantly, this work highlights the potential of such cylindrical micelles to act as biomimetic fibrillar collagen bundles within synthetic extracellular matrix, enabling tunable mechanical properties and antibacterial activities for other biomedical applications, such as antibacterial dressings and packaging.

4 | MATERIALS AND METHODS

4.1 | Materials

Chemicals and solvents were purchased from Sigma-Aldrich, Acros, Fluka, TCI, Fisher Chemical, Alfa Aesar, or VWR. ε-Caprolactone (ε-CL) monomer was distilled over calcium hydride before being stored in a glove box under an inert atmosphere. Diphenyl phosphate (DPP) was recrystallized once from dried $CHCl_3$/Hexane (3:1) and dried over phosphorus pentoxide (P_2O_5) before use. (−)-Sparteine was dried over calcium hydride and distilled before use. 1,4-Dioxane, chloroform, methyl methacrylate (MMA), and 2-(*tert*-butylamino)ethyl methacrylate (TA) were purified by passing through basic alumina before use. 2,2′-Azobis (2-methylpropionitrile) (AIBN) was received from Molekula, recrystallized from methanol, and stored at 4 °C. Deuterated solvents were received from Apollo Scientific.

The bacteria used in this work were gram-positive *S. aureus* (SA01 and SA02 strains) and gram-negative *E. coli* (EC07 and EC19 strains), which were purchased from LGC Standards, Middlesex, UK, and used within a passage window of 30. Liquid Luria-Bertani (LB) medium (final pH 7.4) was purchased from Sigma-Aldrich, which contained the following: 10.0 g tryptone, 5.0 g yeast extract, and 10.0 g sodium chloride.

4.2 | Typical procedure for the ROP of PCL homopolymers

In a nitrogen-filled glove box, solutions of DPP (49 mg, 0.20 mmol) in dry toluene (2 ml) and dual-head CTA (52 mg, 0.21 mmol) in dry toluene (12.4 ml) were added to ϵ-CL (1.44 g, 12.62 mmol). After stirring for 11 h at room temperature, the solution was removed from the glove box, precipitated three times into ice-cold diethyl ether and collected by centrifugation. The resultant yellow polymer was dried under vacuum over phosphorus pentoxide for 2 days. The products were analyzed by SEC chromatograms and it was ensured there were no shoulders or tails in both sides of high- or low-molecular weight before proceeding with RAFT polymerizations and self-assembly. ^{1}H NMR spectroscopy (300 MHz, $CDCl_3$) δ/ppm: 4.06 (t, 100 H, CH_2OCO), 3.65 (t, 2 H, CH_2OH), 2.30 (t, 100 H, $OCOCH_2$), 1.73–1.33 (m, 330 H, $OCO[CH_2]_5OH$), $M_n = 6.5$ kg mol^{-1}, DP = 55. SEC chromatograms (THF, PMMA standard): $M_n = 1.4$ kg mol^{-1}, $M_w = 1.5$ kg mol^{-1}, $Đ_M = 1.06$.

4.3 | Typical procedure for the synthesis of PCL-*b*-PMMA diblock copolymers

PCL_{55} (500 mg, 0.08 mmol), MMA (383 mg, 3.83 mmol), and AIBN (1.26 mg, 7.66×10^{-3} mmol) were dissolved in 1,4-dioxane (1.28 ml) and placed in an ampoule. The solution was then freeze-pump-thawed three times and heated for 5 h at 70 *E. coli*. The reaction was quenched by immersion of the ampoule in the ice bath, and the polymer was precipitated in ice-cold methanol three times before being dried under vacuum and analyzed. ^{1}H NMR (400 MHz, $CDCl_3$) δ/ppm: 4.06 (t, 100 H, CH_2OCO), 3.59 (45 H, $COOCH_3$), 2.30 (t, 100 H, $OCOCH_2$), 1.91–1.81 (2 m, 8 H,

CCH_2, PMMA), 1.72–1.33 (m, 305 H, $OCO[CH_2]_5OH$), 1.02–0.83 (m, 36 H, CH_3, PMMA), M_n = 8.4 kg mol^{-1}, DP = 19. SEC chromatograms (THF, PMMA standard): M_n = 17.6 kg mol^{-1}, M_w = 18.8 kg mol^{-1}, $Đ_M$ = 1.07.

4.4 | Typical procedure for the synthesis of PCL-*b*-PMMA-*b*-PTA triblock copolymers

PCL_{50}-*b*-$PMMA_{20}$ (100 mg, 0.02 mmol), TA (568 mg, 3.06 mmol), and AIBN (0.3 mg, 1.53 × 10^{-3} mmol) were dissolved in 1,4-dioxane (636 μL) and placed in an ampoule. The solution was subjected three times to freeze-pump-thaw cycles and heated for 24 h at 70 °C. The reaction was then quenched by immersion of the ampoule in the ice bath, and the polymer was precipitated in ice-cold methanol three times before being dried under vacuum and analyzed. ^{1}H NMR (400 MHz, $CDCl_3$) δ/ppm: 4.04 (t, 2 H, CH_2OCO), 4.0 (s, 2 H, OCH_2CH_2NH, PTA), 3.75 (t, 2 H, CH_2OH, PMMA), 3.58 (s, 3 H, $COOCH_3$), 3.40 (q, 2 H, CH_3CH_2), 2.80 (s, 2H, CH_2CH_2NH, PTA), 2.28 (t, 2 H, $OCOCH_2$), 2.10–1.70 (m, 9 H, CCH_3 (PCL), $CH_2CH_2CH_2OCO$ (PCL), CCH_2 (PMMA), CCH_2 (PTA)), 1.60 (m, 4 H, $OCO[CH_2]_5OH$), 1.35 (m, 2 H, $OCOC_2H_4CH_2C_2H_4OH$), 1.25 (m, 3 H, CH_2CH_3), 1.15 (s, 9 H, $C[CH_3]_3$, PTA), 1.02–0.83 (m, 3 H, CCH_3, PMMA, PTA), M_n (NMR) = 34.7 kg mol^{-1}, DP = 142. SEC chromatograms (THF, PMMA standard): M_n = 40.8 kg mol^{-1}, M_w = 45.8 kg mol^{-1}, $Đ_M$ = 1.12.

4.5 | Typical crystallization-driven self-assembly method for the self-nucleation of PTA-based block copolymers

As a typical procedure of self-assembly conditions, PCL-*b*-PMMA-*b*-PTA triblock copolymer (30 mg) was added to 6 ml of ethanol (5.0 mg ml^{-1}) in a screw-capped 7 ml vial. The samples were heated to 90 °C without stirring for 4 h before removing from the heating block and cooling to room temperature. Samples were imaged after 2 weeks of aging at room temperature.

4.6 | Sonication of PTA-based cylindrical micelles

Self-nucleated cylindrical micelles prepared by the CDSA of PCL_{55}-*b*-$PMMA_{19}$-*b*-PTA_{142} triblock copolymers in ethanol (5 mg ml^{-1}) were sonicated using a sonic probe at an ice bath (0 °C). Samples was taken at regular intervals and analyzed by TEM. Seed micelles were obtained by 20 min of sonication.

4.7 | Typical gel formation of nanocomposite calcium alginates

Alginate gels were prepared at 1.5 wt% sodium alginate. Before use, sodium alginate (19.9 mg, 0.100 mmol) was heated in the water to 70 °C for 1 h to aid dissolution and cooled to room temperature. Micelles were dispersed in the water for 2 h before stirring with calcium carbonate (5.0 mg, 0.050 mmol), followed by addition to the sodium alginate solution and vortexing for 1 min. After the addition of d-glucono-δ-lactone (GDL) (17.8 mg, 0.100 mmol), the gel was again vortexed for 1 min before incubating at room temperature for 2 days.

4.8 | Typical procedure for the synthesis of PTA homopolymers

Dual-head CTA (20 mg, 0.080 mmol), TA (2276 mg, 16.06 mmol), and AIBN (1.32 mg, 8.03 × 10^{-3} mmol) were dissolved in 1,4-dioxane (4.25 ml) and placed in an ampoule. The solution was subjected three times to freeze-pump-thaw cycles and heated for 24 h at 70 °C. The reaction was then quenched by immersion of the ampoule in the ice bath, and the polymer was precipitated in ice-cold methanol three times before being dried under vacuum and analyzed. ^{1}H NMR (400 MHz, $CDCl_3$) δ/ppm: 4.0 (s, 2 H, OCH_2CH_2NH), 3.40 (q, 2 H, CH_3CH_2), 2.80 (s, 2H, CH_2CH_2NH), 2.28 (t, 2 H, $OCOCH_2$), 2.10–1.70 (CCH_2), 1.25 (m, 3 H, CH_2CH_3), 1.15 (s, 9 H, $C[CH_3]_3$), 1.02–0.83 (m, 3 H, CCH_3), M_n = 14.2 kg mol^{-1}, DP = 141. SEC chromatograms (THF, PMMA standard): M_n = 25.8 kg mol^{-1}, M_w = 30.0 kg mol^{-1}, $Đ_M$ = 1.16.

ACKNOWLEDGMENTS

The China Scholarship Council and the University of Warwick are acknowledged for a Joint Scholarship to Zehua Li. The 111 project, National Science Fund for Distinguished Young Scholars, NSFC (21925505), and Shanghai international scientific collaboration fund (21520710100) are acknowledged for the collaboration research. The authors are grateful to Dr. Jessica Blair and Helen McNeil for access, expert advice, and training in microbiology experiments.

CONFLICT OF INTEREST

The authors declare no conflict of interest.

DATA AVAILABILITY STATEMENT

The data presented in this study are available from the corresponding author upon reasonable request.

AUTHOR CONTRIBUTIONS

Zehua Li: Data curation (lead); methodology (lead); writing – original draft (lead). **Amanda Pearce:** Data curation (supporting); supervision (supporting); writing – original draft (supporting); writing – review and editing (lead). **Jianzhong Du:** Conceptualization (supporting); project administration (supporting); supervision (supporting); writing – review & editing (supporting). **Andrew Dove:** Conceptualization (equal); project administration (lead); supervision (equal); writing – review and editing (supporting). **Rachel K. O'Reilly:** Conceptualization (equal); funding acquisition (supporting); supervision (equal); writing – review & editing (supporting).

ORCID

Andrew P. Dove https://orcid.org/0000-0001-8208-9309

REFERENCES

[1] Y. Hong, Y. Xi, J. Zhang, D. Wang, H. Zhang, N. Yan, S. He, J. Du, *J. Mater. Chem. B* **2018**, *6*(39), 6311.
[2] D. E. Fullenkamp, J. G. Rivera, Y.-K. Gong, K. H. A. Lau, L. He, R. Varshney, P. B. Messersmith, *Biomaterials* **2012**, *33*(15), 3783.
[3] K. A. Juby, C. Dwivedi, M. Kumar, S. Kota, H. S. Misra, P. N. Bajaj, *Carbohydr. Polym.* **2012**, *89*(3), 906.
[4] M. Yadollahi, I. Gholamali, H. Namazi, M. Aghazadeh, *Int. J. Biol. Macromol.* **2015**, *74*, 136.
[5] F. Wahid, C. Zhong, H.-S. Wang, X.-H. Hu, L.-Q. Chu, *Polymer* **2017**, *9*(12), 636.
[6] A. Muñoz-Bonilla, M. Fernández-García, *Prog. Polym. Sci.* **2012**, *37*(2), 281.
[7] J. Chen, F. Wang, Q. Liu, J. Du, *Chem. Commun.* **2014**, *50*(93), 14482.
[8] N. Annabi, D. Rana, E. Shirzaei Sani, R. Portillo-Lara, J. L. Gifford, M. M. Fares, S. M. Mithieux, A. S. Weiss, *Biomaterials* **2017**, *139*, 229.
[9] R. T. C. Cleophas, J. Sjollema, H. J. Busscher, J. A. W. Kruijtzer, R. M. J. Liskamp, *Biomacromolecules* **2014**, *15*(9), 3390.
[10] H. Zazo, C. I. Colino, J. M. Lanao, *J. Controlled Release* **2016**, *224*, 86.
[11] A. Jain, L. S. Duvvuri, S. Farah, N. Beyth, A. J. Domb, W. Khan, *Adv. Healthcare Mater.* **2014**, *3*(12), 1969.
[12] N. M. Milović, J. Wang, K. Lewis, A. M. Klibanov, *Biotechnol. Bioeng.* **2005**, *90*(6), 715.
[13] L. Timofeeva, N. Kleshcheva, *Appl. Microbiol. Biotechnol.* **2011**, *89*(3), 475.
[14] L. Liu, K. Xu, H. Wang, P. K. Jeremy Tan, W. Fan, S. S. Venkatraman, L. Li, Y.-Y. Yang, *Nat. Nanotechnol.* **2009**, *4*(7), 457.
[15] K. Fukushima, J. P. K. Tan, P. A. Korevaar, Y. Y. Yang, J. Pitera, A. Nelson, H. Maune, D. J. Coady, J. E. Frommer, A. C. Engler, Y. Huang, K. Xu, Z. Ji, Y. Qiao, W. Fan, L. Li, N. Wiradharma, E. W. Meijer, J. L. Hedrick, *ACS Nano* **2012**, *6*(10), 9191.
[16] H. Murata, R. R. Koepsel, K. Matyjaszewski, A. J. Russell, *Biomaterials* **2007**, *28*(32), 4870.
[17] M. Inam, J. C. Foster, J. Gao, Y. Hong, J. Du, A. P. Dove, R. K. O'Reilly, *J. Polym. Sci., Part A: Polym. Chem.* **2019**, *57*(3), 255.
[18] S. Lenoir, C. Pagnoulle, M. Galleni, P. Compère, R. Jérôme, C. Detrembleur, *Biomacromolecules* **2006**, *7*(8), 2291.
[19] G. Seyfriedsberger, K. Rametsteiner, W. Kern, *Eur. Polym. J.* **2006**, *42*(12), 3383.
[20] M. Ignatova, S. Voccia, B. Gilbert, N. Markova, D. Cossement, R. Gouttebaron, R. Jérôme, C. Jérôme, *Langmuir* **2006**, *22*(1), 255.
[21] C.-K. Chen, M.-C. Lee, Z.-I. Lin, C.-A. Lee, Y.-C. Tung, C.-W. Lou, W.-C. Law, N.-T. Chen, K.-Y. A. Lin, J.-H. Lin, *Mol. Pharmaceutics* **2019**, *16*(2), 709.
[22] W. Yuan, J. Wei, H. Lu, L. Fan, J. Du, *Chem. Commun.* **2012**, *48*(54), 6857.
[23] M. Schindler, M. J. Osborn, *Biochemistry* **1979**, *18*(20), 4425.
[24] C. Zhang, Y. Zhu, C. Zhou, W. Yuan, J. Du, *Polym. Chem.* **2013**, *4*(2), 255.
[25] J.-M. Thomassin, S. Lenoir, J. Riga, R. Jérôme, C. Detrembleur, *Biomacromolecules* **2007**, *8*(4), 1171.
[26] H. Zuo, D. Wu, R. Fu, *J. Appl. Polym. Sci.* **2012**, *125*(5), 3537.
[27] J. Song, H. Kong, J. Jang, *Chem. Commun.* **2009**, *36*, 5418.
[28] L. MacFarlane, C. Zhao, J. Cai, H. Qiu, I. Manners, *Chem. Sci.* **2021**, *12*(13), 4661.
[29] Z. Li, A. K. Pearce, A. P. Dove, R. K. O'Reilly, *Polymer* **2021**, *13*(13), 2202.
[30] K. Y. Lee, D. J. Mooney, *Prog. Polym. Sci.* **2012**, *37*(1), 106.
[31] M. C. Arno, M. Inam, Z. Coe, G. Cambridge, L. J. Macdougall, R. Keogh, A. P. Dove, R. K. O'Reilly, *J. Am. Chem. Soc.* **2017**, *139*(46), 16980.
[32] A. Muñoz-Bonilla, M. Cerrada, M. Fernández-García, A. Kubacka, M. Ferrer, M. Fernández-García, *Int. J. Mol. Sci.* **2013**, *14*(5), 9249.
[33] J. B. Gilroy, T. Gädt, G. R. Whittell, L. Chabanne, J. M. Mitchels, R. M. Richardson, M. A. Winnik, I. Manners, *Nat. Chem.* **2010**, *2*(7), 566.
[34] Y. He, J.-C. Eloi, R. L. Harniman, R. M. Richardson, G. R. Whittell, R. T. Mathers, A. P. Dove, R. K. O'Reilly, I. Manners, *J. Am. Chem. Soc.* **2019**, *141*(48), 19088.
[35] K. Zhang, H. Fang, Z. Wang, J.-S. A. Taylor, K. L. Wooley, *Biomaterials* **2009**, *30*(5), 968.
[36] C. K. Kuo, P. X. Ma, *Biomaterials* **2001**, *22*(6), 511.
[37] F. Nederberg, Y. Zhang, J. P. K. Tan, K. Xu, H. Wang, C. Yang, S. Gao, X. D. Guo, K. Fukushima, L. Li, J. L. Hedrick, Y.-Y. Yang, *Nat. Chem.* **2011**, *3*(5), 409.
[38] D. I. Chan, E. J. Prenner, H. J. Vogel, *Biochim. Biophys. Acta, Biomembr.* **2006**, *1758*(9), 1184.
[39] Z. V. Feng, I. L. Gunsolus, T. A. Qiu, K. R. Hurley, L. H. Nyberg, H. Frew, K. P. Johnson, A. M. Vartanian, L. M. Jacob, S. E. Lohse, M. D. Torelli, R. J. Hamers, C. J. Murphy, C. L. Haynes, *Chem. Sci.* **2015**, *6*(9), 5186.

SUPPORTING INFORMATION

Additional supporting information may be found in the online version of the article at the publisher's website.

How to cite this article: Z. Li, A. K. Pearce, J. Du, A. P. Dove, R. K. O'Reilly, *J. Polym. Sci.* **2022**, 1. https://doi.org/10.1002/pol.20210853